

1 **Combination of cuprizone and experimental autoimmune encephalomyelitis to study**
2 **inflammatory brain lesion formation and progression**

3
4 Bernhard Josef Rüter¹, Miriam Scheld¹, Daniela Dreymueller², Tim Clarner¹, Eugenia Kress³, Lars-
5 Ove Brandenburg³, Tine Swartenbroekx⁴, Chloé Hoornaert⁴, Peter Ponsaerts⁴, Petra Fallier-Becker⁵,
6 Cordian Beyer¹, Sven Olaf Rohr⁶, Christoph Schmitz⁶, Uta Chrzanowski⁶, Tanja Hochstrasser⁶, Stella
7 Nyamoya^{1,6}, and Markus Kipp⁶
8

9 ¹Institute of Neuroanatomy and JARA-BRAIN, Faculty of Medicine, RWTH Aachen University, 52074
10 Aachen, Germany

11 ²Institute of Pharmacology and Toxicology, Faculty of Medicine, RWTH Aachen University, 52074
12 Aachen, Germany

13 ³Department of Anatomy and Cell Biology, RWTH Aachen University, 52074 Aachen, Germany

14 ⁴Faculty of Medicine and Health Sciences, University of Antwerp, 2610 Antwerp, Belgium

15 ⁵Institute of Pathology and Neuropathology, University of Tuebingen, 72076 Tuebingen, Germany

16 ⁶Department of Anatomy II, Ludwig-Maximilians-University of Munich, 80336 Munich, Germany
17

18 **Corresponding author:**

19 Markus Kipp

20 Anatomische Anstalt; Lehrstuhl II - Neuroanatomie

21 Pettenkoferstr. 11; 80336 München

22 mail: markus.kipp@med.uni-muenchen.de
23

24 **Funding information:** Dr. Robert Pflieger Stiftung
25

26 **Main points:**

27 1. Cuprizone-induced cytodeneration triggers monocyte, lymphocyte, and granulocyte recruitment
28 into the forebrain.

29 2. Peripheral immune cell recruitment induces acute axonal injury.

30 3. Cytodeneration augments cerebellar inflammation in experimental autoimmune encephalomyelitis.
31

32 **Keywords:** cuprizone, EAE, inflammation, multiple sclerosis
33

34 **Abstract**

35 Brain-intrinsic degenerative cascades are a proposed factor driving inflammatory lesion formation in
36 multiple sclerosis (MS) patients. We recently described a model combining noninflammatory
37 cytodeneration (via cuprizone) with the classic active experimental autoimmune encephalomyelitis

38 (Cup/EAE model), which exhibits inflammatory forebrain lesions. Here, we describe the
39 histopathological characteristics and progression of these Cup/EAE lesions. We show that inflammatory
40 lesions develop at various topographical sites in the forebrain, including white matter tracts and cortical
41 and subcortical grey matter areas. The lesions are characterized by focal demyelination, discontinuation
42 of the perivascular glia limitans, focal axonal damage, and neutrophil granulocyte extravasation.
43 Transgenic mice with enhanced green fluorescent protein-expressing microglia and red fluorescent
44 protein-expressing monocytes reveal that both myeloid cell populations contribute to forebrain
45 inflammatory infiltrates. EAE-triggered inflammatory cerebellar lesions were augmented in mice pre-
46 intoxicated with cuprizone. Gene expression studies suggest roles of the chemokines *Cxcl10*, *Ccl2*, and
47 *Ccl3* in inflammatory lesion formation. Finally, follow-up experiments in Cup/EAE mice with chronic
48 disease revealed that forebrain, but not spinal cord, lesions undergo spontaneous reorganization and
49 repair. This study underpins the significance of brain-intrinsic degenerative cascades for immune cell
50 recruitment and, in consequence, MS lesion formation.

51

52 **Introduction**

53 Multiple sclerosis (MS) is a neuroinflammatory disorder of the central nervous system (CNS) with a
54 high prevalence, especially in young adults. MS lesions are characterized by oligodendrocyte death,
55 demyelination, gliosis, axonal damage, and peripheral immune cell infiltration (Bauer, Rauschka, &
56 Lassmann, 2001; Benn, Halfpenny, & Scolding, 2001). MS is a clinically heterogeneous disorder that
57 presents as a relapsing-remitting, secondary progressive, or primary progressive form (Lublin et al.,
58 2014). Relapsing-remitting MS involves episodes or “attacks” of varied symptoms, including
59 disturbances in vision and balance, dizziness, fatigue, incontinence, pain, muscle weakness or spasticity,
60 and cognitive impairment. The frequency and severity of inflammatory attacks vary from patient to
61 patient. In severe cases (i.e. Marburg's variant of MS), inflammatory demyelination can lead to severe
62 functional deficits and sometimes death (Nunes et al., 2015; Rush, MacLean, & Freedman, 2015). Some
63 cases of MS are more benign, with no worsening of functional ability, even after 15 years of diagnosis,
64 and low annualized relapse rates (Glad, Nyland, Aarseth, Riise, & Myhr, 2009; Sartori, Abdoli, &
65 Freedman, 2017). However, in most cases, these attacks can recur with increasing frequency and proceed
66 to secondary progressive MS, which, as with primary progressive forms, involves axonal damage and
67 neurodegeneration (Charcot, 1868; Kornek et al., 2000; Trapp, Ransohoff, & Rudick, 1999) resulting in
68 irreversible clinical disability. Despite decades of research, it is still not clear whether immune
69 dysregulation or intrinsic cytodenerative events are responsible for the formation of new lesions
70 (Barnett & Prineas, 2004; Codarri, Greter, & Becher, 2013).

71 We recently demonstrated that primary oligodendrocyte degeneration can trigger peripheral
72 immune cell recruitment into the forebrain (Scheld et al., 2016). In that study, oligodendrocyte apoptosis
73 in the forebrains of mice was first induced by a 3-week treatment with cuprizone, and an infiltration of
74 myelin autoreactive T cells from peripheral lymphoid organs was then triggered by experimental

75 autoimmune encephalomyelitis (EAE) via immunization with the myelin oligodendrocyte glycoprotein
76 35–55 peptide (MOG_{35–55}) (Iglesias, Bauer, Litzemberger, Schubart, & Linington, 2001). Our work and
77 those of others (Baxi et al., 2015; Boretius et al., 2012) clearly illustrate the significance of brain-
78 intrinsic degenerative cascades for immune cell recruitment and MS lesion formation.

79 The purpose of this study was to characterize the histopathology of inflammatory foci in our
80 cuprizone-EAE model. Specifically, we sought to determine the composition of inflammatory infiltrates,
81 which can include T lymphocytes and macrophages (Lucchinetti et al., 2000), as well as activated
82 astrocytes and microglia and neutrophil granulocytes (Hertwig et al., 2016). We found that fluorescently
83 labeled microglia and monocytes are both present in inflammatory lesions, with gene expression studies
84 implicating the involvement of the chemokines C-X-C motif ligand 10 (CXCL10), C-C motif ligand 2
85 (CCL2), and C-C motif ligand 3 (CCL3) in inflammatory lesion formation. Finally, follow-up
86 experiments revealed that, unlike spinal cord lesions, forebrain lesions exhibit spontaneous
87 reorganization and repair.

88

89 **Materials and Methods**

90 *Animals and experimental groups*

91 C57BL/6 mice (Janvier Labs, Le Genest-Saint-Isle, France) were bred and maintained at a maximum of
92 five animals per cage with *ad libitum* food and water in a pathogen-free environment. Cages were
93 cleaned once per week and microbiological monitoring was performed according to the Federation of
94 European Laboratory Animal Science Associations recommendations. Female 10-week-old (19–21 g)
95 mice were randomly assigned to four groups (Fig. 1A): (i) control, animals received a diet of standard
96 rodent chow for the duration of the 7-week study; (ii) cuprizone (Cup), animals were fed a diet
97 containing 0.25% cuprizone [bis(cyclohexanone)oxaldihydrazone; Sigma-Aldrich Inc., St Louis, MO,
98 USA] mixed into ground standard rodent chow for three weeks, followed by four weeks of normal chow;
99 (iii) Cup/EAE, mice were fed the cuprizone diet for the first three weeks and were then immunized with
100 MOG_{35–55} at the beginning of week six; (iv) EAE, animals received the standard rodent chow for the
101 duration of the study but were immunized with MOG_{35–55} at the beginning of week six. An additional
102 cohort of Cup/EAE animals was used to investigate inflammatory brain lesions during chronic disease,
103 47 days after immunization. A second study utilized female CX₃CR1^{+eGFP}/CCR2^{+RFP} reporter gene
104 transgenic mice [C57BL/6 background; (Dooley et al., 2016; Le Blon et al., 2016)] with green
105 fluorescent microglia and red fluorescent infiltrating macrophages/monocytes under the same
106 experimental conditions to discriminate brain-resident microglia from infiltrating peripheral
107 monocytes/macrophages.

108

109 *EAE and disease scoring*

110 To induce the formation of myelin autoreactive T cells, mice were immunized with an injection of an
111 emulsion of MOG_{35–55} peptide dissolved in complete Freund's adjuvant followed by injections of

112 pertussis toxin in PBS on the day of and the day after immunization (Hooke Laboratories, USA). Disease
113 severity was scored as follows: 1, the entire tail drapes over the observer's finger when the mouse is
114 picked up by base of the tail; 2, the legs are not spread apart but held close together when the mouse is
115 picked up by base of the tail, and mice exhibit a clearly apparent wobbly gait; 3, the tail is limp and mice
116 show complete paralysis of hind legs (a score of 3.5 is given if the mouse is unable to raise itself when
117 placed on its side); 4, the tail is limp and mice show complete hind leg and partial front leg paralysis,
118 and the mouse is minimally moving around the cage but appears alert and feeding (a score of 4 was not
119 attained by any of the mice in our study).

120

121 *Tissue preparation*

122 For histological and immunohistochemical studies, mice were anaesthetized with ketamine (100
123 mg·kg⁻¹ i.p.) and xylazine (10 mg·kg⁻¹ i.p.) and transcardially perfused with ice-cold PBS followed by
124 a 3.7% paraformaldehyde solution (PFA; pH 7.4). Brains were postfixed overnight in PFA, dissected,
125 embedded in paraffin, and then coronal sections (5 µm) were cut (Acs et al., 2009; Clarner et al., 2012).
126 Spinal cords were incubated in EDTA (ethylenediaminetetraacetic acid) solutions for 48 h (changed
127 once) at 37°C prior to paraffin embedding. This decalcification procedure was not performed for
128 samples from some EAE mice to enable the enzymatic detection of neutrophils. For gene expression
129 studies, tissues were manually dissected after transcardial PBS perfusion, immediately frozen in liquid
130 nitrogen, and kept at -80°C until further processing. For ultrastructural analyses by electron microscopy,
131 tissue preparation was performed according to protocols published previously by our laboratory
132 (Norkute et al., 2009).

133

134 *Immunohistochemistry and neutrophil staining*

135 For immunohistochemistry, sections were rehydrated and, if necessary, antigens were unmasked with
136 Tris/EDTA buffer (pH 9.0) or citrate (pH 6.0) heating. After washing in PBS, sections were incubated
137 overnight (4°C) with the following primary antibodies diluted in blocking solution (serum of species in
138 which the secondary antibody was produced). Anti-gial fibrillary acidic protein antibody ([GFAP]
139 1:12,000; EnCor Biotechnologie Inc, Gainesville, FL, USA) was used to visualize astrocytes, anti-
140 ionized calcium-binding adaptor molecule 1 antibody ([Iba1] 1:10,000; Wako Chemicals GmbH, Neuss,
141 Germany) was used to detect microglia/macrophages, and anti-amyloid precursor protein antibody
142 ([APP] 1:5,000, Merck-Millipore) was used to detect acute axonal damage (Bitsch, Schuchardt,
143 Bunkowski, Kuhlmann, & Bruck, 2000; Gehrman, Banati, Cuzner, Kreutzberg, & Newcombe, 1995;
144 Kuhlmann, Lingfeld, Bitsch, Schuchardt, & Bruck, 2002; Pfeifenbring et al., 2015; Schirmer, Merkle,
145 König, Bruck, & Stadelmann, 2013). The next day, slides were incubated with biotinylated secondary
146 antibodies for 1 h and then with peroxidase-coupled avidin-biotin complex (ABC kit; Vector
147 Laboratories, Peterborough, UK) and treated with 3,3'-diaminobenzidine (DAKO, Hamburg, Germany)
148 as a peroxidase substrate or incubated with Alexa Fluor-coupled secondary antibodies (Life

149 Technologies, Germany) as published previously (Hoflich et al., 2016). Luxol fast blue (LFB)/periodic
150 acid-Schiff stains were performed following established protocols. To visualize granulocytes in
151 paraffin-embedded tissues, a naphthol AS-D chloroacetate (specific esterase) kit was used (Sigma-
152 Aldrich, Germany).

153 Stained and processed sections were digitalized using a Nikon ECLIPSE E200 microscope
154 (Nikon, Nikon Instruments, Düsseldorf, Germany) equipped with a DS-Vi1 camera. To analyze
155 microglia/monocyte densities in the cerebelli, Iba1 immunoreactivity was scored as ranging from 1
156 (baseline “normal” reactivity) to 5 (maximum reactivity) by two evaluators blinded to the treatment
157 groups, and the results were averaged. The open source program ImageJ (NIH, Bethesda, MD, USA)
158 was used to determine cellular densities and to quantify the numbers of APP⁺ spheroids at specified
159 distances from inflamed vessels. To quantify the numbers and localization of perivascular infiltrates in
160 the forebrain and cerebellum, lesions were identified in hematoxylin and eosin (H&E)-stained sections
161 by two evaluators blinded to the treatment groups, and the results were averaged. Forebrains were
162 analyzed at the levels R235 and R275 according to the mouse brain atlas by Sidman et al.
163 (<http://www.hms.harvard.edu/research/brain/atlas.html>), whereas cerebelli were analyzed at the levels
164 R465 and R485.

165

166 *Discrimination of microglia and recruited monocytes in CX₃CR1^{+eGFP}/CCR2^{+RFP} mice*

167 All immunofluorescence analyses were performed according to previously described procedures
168 (Dooley et al., 2016; Le Blon et al., 2016). Briefly, mice were transcardially perfused with a 0.9% NaCl
169 solution followed by 4.0% PFA. Next, brains were isolated, further fixed in 4.0% PFA for 3 h, and then
170 protected through a gradient of 5%, 10%, and 20% sucrose. Afterwards, brain tissue was snap-frozen in
171 liquid nitrogen and kept at -80°C until further processing. Cryosections (10 µm) were cut using an
172 HM500 cryostat and incubated first with a rabbit anti-RFP antibody (2.5 µg/mL, ab62341; Abcam) and
173 then a secondary donkey anti-rabbit Alexa Fluor 555 antibody (2 µg/mL, A31572; Invitrogen). Nuclear
174 staining was performed using TO-PRO-3 (1:200; Life Technologies) and sections were mounted with
175 Prolong Gold anti-fading reagent. Images were acquired using a BX51 fluorescence microscope
176 equipped with an Olympus DP71 digital camera and processed with Olympus cellSens dimension
177 software. Quantitative analysis of eGFP⁺ brain-resident microglia and infiltrating RFP⁺ peripheral
178 monocytes/macrophages was performed using the TissueQuest immunofluorescence analysis software
179 (v3.0; TissueGnostics GmbH). After manually delineating the region of interest (midline of the corpus
180 callosum) using ImageJ, the total numbers of TO-PRO-3⁺ nuclei and those colocalizing with a direct
181 eGFP fluorescence signal and/or antibody-stained anti-RFP fluorescence signal were automatically
182 determined using TissueQuest software. Each staining/analysis was performed in duplicate.

183 *Transmission electron microscopy*

184 Tissue samples were fixed with 2.5% glutaraldehyde (Science Services, Munich, Germany) in
185 cacodylate buffer (pH 7.4; Merck-Millipore, Darmstadt, Germany) at 4°C overnight as described
186 previously (Noell et al., 2012). Thereafter, samples were embedded in Araldite (Serva, Heidelberg,
187 Germany), and ultrathin sections were cut using a Leica ultramicrotome (Leica, Wetzlar, Germany) and
188 analyzed using a Zeiss EM-10 transmission electron microscope (Zeiss, Oberkochen, Germany).

189

190 *Gene expression analyses*

191 Gene expression levels were measured by real-time reverse transcription-PCR ([qRT-PCR] Bio-Rad,
192 Munich, Germany) using SensiMix Plus SYBR and fluorescein (Quantace, Bionline, Luckenwalde,
193 Germany) with a standardized protocol as described previously by our group (Slowik et al., 2015).
194 Primer sequences and individual annealing temperatures are shown in Table 1. Relative quantification
195 was performed using the $\Delta\Delta C_t$ method with β actin as the reference gene. Melting curves and gel
196 electrophoresis of the PCR products were routinely performed to determine the specificity of the PCR
197 reactions (data not shown).

198

199 *Flow cytometry analysis of primary blood cells*

200 Peripheral blood samples (400 μ L, citrated 0.38%) were subjected to erythrocyte lysis (155 mM NH_4Cl ,
201 10 mM NaHCO_3 , 5 mM EDTA, pH 7.4) and resuspended in assay buffer (PBS with 1% fetal bovine
202 serum and 1 mM EDTA); all steps of the staining process were performed at 4°C. Prior to staining for
203 forkhead box P3 (FOXP3) and interferon γ , cells were first permeabilized with 0.1% Triton-X 100 in
204 PBS. For cell surface staining the differentiation of T-helper cell subsets, blood samples were stained
205 with anti-CD4-allophycocyanin-H7, anti-CD25-allophycocyanin, anti-IL17A, and FOXP3-fluorescein
206 (BD Pharmingen), and anti-interferon γ -PB (eBioscience). For the differentiation of leukocyte subsets,
207 samples were stained with anti-Ly6G-allophycocyanin (Miltenyi Biotec), anti-F4/80-phycoerythrin
208 (Serotec), anti-CD4-allophycocyanin-H7, and anti-CD8-PB (BD Pharmingen). Samples were analyzed
209 using a FACS LSR Fortessa (BD Biosciences) with FlowJo software.

210

211 *Statistical analysis*

212 Statistical analyses were performed using Prism 5 (GraphPad Software Inc., San Diego, CA, USA). All
213 data are given as arithmetic means \pm SEMs. A p value of <0.05 was considered to be statistically
214 significant.

215

216 **Results**

217 *Clinical progression of symptoms in Cup/EAE and EAE mice*

218 As expected, control and cuprizone-intoxicated mice did not show any clinical signs of disease.
219 However, EAE and Cup/EAE mice exhibited signs of disease progression beginning ~11 days after

220 immunization (10.8 ± 0.58 vs. 11.0 ± 0.31 days; $p = 0.77$) (Fig. 1B). There was no difference between
221 these groups in the average maximum disease score (2.3 ± 0.34 vs. 2.8 ± 0.25 ; $p = 0.27$). In line with
222 these observations, the histopathological appearance of spinal cord tissues (Fig. 1C) and the numbers of
223 spinal inflammatory infiltrates (Fig. 1D) were comparable in Cup/EAE and EAE animals. Such lesions
224 were present at several topographical sites, including the ventral, lateral, and dorsal funiculi, with all
225 segments (i.e., cervical, thoracic, lumbar, and sacral) of the spinal cord affected equally.

226

227 *Distribution of inflammatory forebrain lesions*

228 As previously described (Scheld et al., 2016), focal inflammatory infiltrates in our model are
229 characterized by perivascular immune cell accumulation (i.e., within an enlarged Virchow-Robin space),
230 perivascular astrogliosis, and demyelination (see Fig. 2A). Recruited inflammatory cells frequently
231 progressed through the astrocytic glia limitans perivascularis to invade the surrounding neuropil. GFAP
232 immunoreactivity was increased around the lesions, and focal demyelination was pronounced in lesions
233 where peripheral immune cells had invaded the perivascular neuropil. H&E stains were performed to
234 visualize the number and distributions of these lesions in brain sections at two levels of the forebrain
235 from animals sacrificed at the peak of the disease (i.e., at day 14 postimmunization) (Fig. 2B). Loci of
236 perivascular infiltrates were absent in the brains of control and cuprizone-intoxicated animals, and there
237 were few in EAE-immunized animals that were primarily periventricular. By contrast, many loci of
238 perivascular infiltrates were present in Cup/EAE animals, and these lesions were widely distributed
239 throughout the corpus callosum and cortical and subcortical grey matter areas.

240 To test for the presence of acute axonal injury around inflammatory infiltrates, lesions were
241 identified in H&E-stained slides and adjacent sections were stained for APP, a well-known marker for
242 acute axonal injury (Hoflich et al., 2016). Under pathological conditions, anterograde axonal transport
243 is disturbed and APP accumulates as ovoid spheroids (Kuhlmann et al., 2002). Therefore, we measured
244 the densities of APP⁺ spheroids in concentric areas around the vessel centers. As shown in Fig. 2C,
245 spheroid densities were highest in the immediate vicinity of the inflamed vessel and progressively
246 declined with increasing distance. This result led us to conclude that inflammatory infiltrating
247 peripheral immune cells, either lymphocytes or monocytes, focally induce acute axonal injury.

248

249 *Characterization of inflammatory response*

250 The composition of peripheral inflammatory cells was determined via flow cytometry analysis of blood
251 samples collected during the peak phase of the disease (i.e., directly before the animals were sacrificed).
252 EAE and Cup/EAE mice had higher numbers of total leucocytes (Fig. 3A), neutrophils (Fig. 3B), CD4⁺
253 lymphocytes (Fig. 3C), and monocytes (F4/80⁺ cells; Fig. 3D) than controls and Cup mice. For a more
254 fine-grained analysis, we further quantified the total numbers of CD4⁺CD25⁺FOXP3⁺ regulatory T cells
255 and CD4⁺Th17⁺ effector T cells in peripheral blood. In line with reported findings (Korn et al., 2007;
256 McGeachy, Stephens, & Anderton, 2005), the numbers of regulatory T cells were comparable in control,

257 cuprizone, and EAE mice, whereas a significant induction was observed in Cup/EAE mice (Fig. 3E).
258 Whereas the numbers of Th17 effector T cells were slightly increased in Cup and EAE mice, there was
259 a significant induction in Cup/EAE mice (Fig. 3F). As flow cytometry revealed a higher number of
260 neutrophils in Cup/EAE animals, and other studies in EAE indicate that neutrophils have an important
261 role in inflammation (Y. Liu et al., 2015; Pierson, Wagner, & Goverman, 2016), we examined
262 ultrastructural as well as enzymatically stained images to identify neutrophils in perivascular infiltrates
263 (Fig. 3G). Using both techniques, high numbers of neutrophils were found in the perivascular
264 compartment and in the forebrain parenchyma, with densities of ranging from 1,778 to 12,526 cells/mm²
265 (mean, 4,614 ± 359 granulocytes/mm²) in the proximity of perivascular forebrain lesions. As shown in
266 Fig. 3G (lower right), the density of neutrophil granulocytes in perivascular forebrain lesions of
267 Cup/EAE mice was comparable to that found in the spinal cords of EAE mice (4,614 ± 359 cells/mm²
268 vs. 3,647 ± 357.5 granulocytes/mm²; $p = 0.083$).

269

270 *Microglia activation and Monocyte recruitment in Cup/EAE animals*

271 The activation of microglia and recruitment of monocytes in sites of demyelination that are characteristic
272 of MS lesions are not observed in the cuprizone mouse model (McMahon, Suzuki, & Matsushima,
273 2002). To determine if these occur in our Cup/EAE model, we utilized transgenic
274 (CX₃CR1^{+eGFP}/CCR2^{+RFP}) mice with eGFP-expressing microglia and RFP-expressing monocyte-
275 derived macrophages (Saederup et al., 2010). The numbers of forebrain eGFP⁺ microglia were within
276 the physiological range in control and EAE mice but significantly increased in Cup and Cup/EAE mice
277 (Fig. 4A,B). By contrast, numbers of RFP⁺ monocyte-derived macrophages were only significantly
278 elevated in Cup/EAE mice. These results clearly demonstrate that, whereas forebrain microglial
279 activation is not characteristic of the EAE model, significantly more microglia as well as monocytes are
280 recruited to the forebrain lesions of Cup/EAE mice.

281

282 *Peripheral immune cell recruitment is paralleled by the induction of adhesion molecules*

283 We next analyzed the expression of genes encoding cell adhesion molecules in the corpus callosa of
284 experimental mice. To validate this method, we compared the quantification of GFAP⁺ reactive
285 astrocytes by immunohistochemistry with transcript levels by qRT-PCR. Both methods revealed similar
286 significant increases in GFAP in Cup and Cup/EAE animals compared with control mice (Fig. 5A).
287 Therefore, we measured the transcript levels of intercellular adhesion molecule 1 (*Icam1*) and vascular
288 cell adhesion molecule 1 (*Vcam1*) in our experimental groups. Strikingly, both were significantly
289 increased only in Cup/EAE mice (Fig. 5B).

290

291 *Cuprizone intoxication augments cerebellar immune cell infiltration*

292 In the forebrain, the interplay between innate immune activation (via cuprizone intoxication) and
293 adaptive immunity (via EAE) is used to model MS disease activity. As both models also impact the

294 cerebellum (Groebe et al., 2009; Skripuletz et al., 2010), we investigated this region to determine
295 whether changes are augmented in our Cup/EAE model. Similar to what we observed in the forebrain,
296 there were many loci of perivascular infiltrates in the cerebella of Cup/EAE mice, and virtually none in
297 control and Cup mice, as well as in cuprizone-treated mice “immunized” with complete Freund’s
298 adjuvant and pertussis toxin only (lacking the MOG₃₅₋₅₅ peptide) (Fig. 6A). Although a moderate
299 number of loci were present in EAE mice, significantly more were detected in Cup/EAE mice (10 ± 2.1
300 vs. 32 ± 4.3 loci per slide; $p = 0.008$), and could be found in the cerebellar cortex, arbor vitae and deep
301 cerebellar white matter, and in the adjacent brainstem. To determine if this peripheral immune cell
302 recruitment in the cerebellum is paralleled by an increase in microglia/monocyte activity, we performed
303 immunohistochemistry for the microglia/monocyte pan-marker Iba1, and staining intensity was
304 quantified by visual scoring (1–5; see Fig. 6C,D). The cerebella of Cup and EAE mice showed an
305 expected increase in microglia/monocyte reactivity, whereas the increase was significantly higher in
306 Cup/EAE mice.

307

308 *Increased chemokine expression in Cup/EAE mice.*

309 As chemokines have a central role in orchestrating innate and adaptive immune responses (Hartung,
310 Aktas, Menge, & Kieseier, 2014), we assessed the expression of *Cxcl10*, *Ccl2*, and *Ccl3* in the corpus
311 callosa, cerebella, and spinal cords of experimental mice. *Cxcl10* levels were significantly increased in
312 the cerebella and spinal cords of EAE mice, and were significantly higher in all three areas in Cup/EAE
313 mice (Fig. 7A). A similar expression pattern was observed for *Ccl2* (Fig. 7B). Of note, expression
314 patterns for *Ccl3* differed among the regions. In the spinal cord, the pattern of *Ccl3* expression was
315 similar to those of *Cxcl10* and *Ccl2*, with a significant increase over controls in the EAE group and even
316 higher expression in Cup/EAE mice. However, in the corpus callosum and cerebellum, *Ccl3* expression
317 was significantly induced in Cup and Cup/EAE mice; no induction was observed in EAE mice. These
318 results demonstrate a region- and chemokine-specific induction of inflammatory cytokines.

319

320 *Repair of inflammatory forebrain lesions*

321 To examine the progression of inflammatory forebrain lesions in Cup/EAE mice, we sacrificed a cohort
322 of animals approximately 7 weeks after MOG₃₅₋₅₅ immunization (i.e., the chronic group) (Fig. 8A). After
323 the peak of clinical disease, clinical scores in Cup/EAE animals abated somewhat but the animals
324 remained clinically impaired until the end of the observation period (Fig. 8B). To verify that these
325 clinical scores reflect the extent of inflammation in the spinal cord, we examined the histopathology of
326 the spinal cords. In line with our behavioral observations, inflammatory demyelination within the spinal
327 cord white matter of Cup/EAE animals was still present during the chronic stage. In LFB/periodic acid-
328 Schiff stained sections, ~5.3% of the entire white matter was affected in chronic Cup/EAE groups,
329 comparable to the 4.4% affected in Cup/EAE mice at the peak of clinical disease (~2 weeks after
330 immunization in the “acute” group). However, chronic lesions were less inflammatory than acute

331 lesions, but showed marked loss of LFB staining (Fig. 8C). This difference in LFB staining intensity
332 was not due to differences in tissue processing during the staining procedure. Thus, the spinal cord
333 pathology remained stable during chronic disease. Next, we investigated the forebrains at distinct rostral
334 to caudal levels for the presence of inflammatory infiltrates during chronic disease. To our great surprise,
335 there were substantially fewer inflammatory infiltrate foci in forebrains of animals sacrificed during the
336 chronic stage than in those sacrificed at the acute stage (Fig. 8D). The majority of lesions were found
337 around the third ventricle and within the striatum.

338

339 **Discussion**

340 We recently developed a novel MS animal model characterized by multifocal inflammatory forebrain
341 lesions (Scheld et al., 2016). In this study, we characterized these lesions at the cellular level and found
342 that they are dominated by microglia and infiltrating monocytes. Specifically, our results show (i) that
343 in the cuprizone model, peripheral monocyte recruitment is not a dominant feature, (ii) that the corpus
344 callosum is not a predilection site in MOG₃₅₋₅₅-induced EAE, and (iii) that brain-intrinsic degenerative
345 processes induced by cuprizone support the opening of the blood-brain-barrier (BBB) and facilitate the
346 recruitment of peripheral monocytes to the lesion sites (Alvarez, Katayama, & Prat, 2013).

347 The integrity of the BBB and the contribution of peripheral immune cells to cuprizone-induced
348 pathology is controversial in the literature. After cuprizone-induced acute demyelination, no BBB
349 disruption has been detected by horseradish peroxidase tracing or immunohistochemical staining for
350 serum proteins, despite robust microglial and astrocytic responses (Bakker & Ludwin, 1987; Kondo,
351 Nakano, & Suzuki, 1987). Moreover, gadolinium magnetic resonance imaging in mice did not reveal a
352 disturbance of BBB integrity after 5 weeks of cuprizone intoxication (Boretius et al., 2012).
353 Histologically, these lesions did not exhibit deposition of immunoglobulins or fibrinogen, markers of
354 lost BBB integrity. In contrast to these data, a recent report demonstrated extravasation of Evans blue
355 dye into the CNS of cuprizone-fed mice, indicating minor loss of BBB integrity (Berghoff et al., 2017).
356 In addition, a study by McMahon and colleagues (McMahon et al., 2002) showed that a small number
357 of peripheral macrophages do indeed migrate into the brain in response to cuprizone-induced
358 demyelination. However, their study involved brain irradiation to generate the GFP bone marrow
359 chimeric mice, a treatment that was suggested to be responsible for the observed effect (Mildner et al.,
360 2007). Furthermore, recombination activating gene 1 (RAG1)-deficient mice that lack T and B cells are
361 fully vulnerable to cuprizone-induced demyelination, indicating that T and B cells are not required or
362 involved in this model (Hiremath, Chen, Suzuki, Ting, & Matsushima, 2008). Nevertheless, early and
363 transient recruitment of C-X-C motif chemokine receptor 2-expressing neutrophils has been implicated
364 in cuprizone-induced demyelination (L. Liu et al., 2010). Overall, the results from most studies suggest
365 that peripheral immune cells have negligible significance in cuprizone-induced pathology, which instead
366 is characterized by microglia accumulation. Consistent with this, we observed a significant increase in
367 microglia in Cup mice.

368 Inflammatory lesions in MOG₃₅₋₅₅-induced EAE are primarily observed in the spinal cord,
369 cerebellum, and optic nerve (Kuerten et al., 2007; Scheld et al., 2016). Our data show that cuprizone
370 intoxication permits involvement of the forebrain in EAE. We hypothesize that this occurs via a three-
371 step process. First, cuprizone activates cells of the BBB (i.e. astrocytes, pericytes, and endothelial cells),
372 compromising its integrity. Second, encephalitogenic immune cells invade the forebrain parenchyma
373 and are locally reactivated. Third, a secondary wave of immune cell recruitment results in the
374 inflammatory demyelinating lesions. Thus, there must be identifiable factors in Cup/EAE mice that
375 contribute to these steps.

376 We found that the expression of specific cell adhesion molecules was induced exclusively in
377 Cup/EAE mice, suggesting that these treatments have produced an environment conducive to
378 inflammatory cell activity. Moreover, we identified upregulation of *Ccl2*, *Ccl3*, and *Cxcl10*, which
379 encode chemokines that act as chemoattractants for various inflammatory cells, including T
380 lymphocytes (Carr, Roth, Luther, Rose, & Springer, 1994; K. K. Liu & Dorovini-Zis, 2012; Millward,
381 Caruso, Campbell, Gauldie, & Owens, 2007), dendritic cells (Xu, Warren, Rose, Gong, & Wang, 1996),
382 monocytes (Moreno et al., 2014; Price et al., 2014), and microglia (Clarner et al., 2015; Moreno et al.,
383 2014). Interestingly, the cerebella of mice showed relatively weaker induction of these chemokines,
384 despite that obvious involvement of this region in EAE by our work and those of others. For instance,
385 the induction of *Ccl3* expression is moderate in the cerebella of EAE-diseased mice. Thus, it is possible
386 that distinct chemokines regulate peripheral immune cell recruitment in particular brain regions. A
387 clearer understanding of this is of vital importance for developing future therapeutic anti-chemokine
388 strategies. If, for example, CCL3 regulates inflammation in the brain but not in the cerebellum, patients
389 with greater forebrain involvement would benefit from anti-chemokine strategies that target CCL3.

390 Myeloid cells predominate in active MS brain lesions (Lucchinetti et al., 2000; Werner, Bitsch,
391 Bunkowski, Hemmerlein, & Bruck, 2002), and recently, the neutrophils have increasingly become the
392 focus of EAE studies where they migrate from the blood into the spinal cord parenchyma early during
393 the disease course (Aube et al., 2014; Wu, Cao, Yang, & Liu, 2010). Indeed, the recruitment of
394 neutrophils is an early and transient event (Aube et al., 2014; Wu et al., 2010), and depletion delays the
395 clinical manifestation of EAE and prevents disruption of the blood-spinal cord-barrier (Aube et al., 2014;
396 Steinbach, Piedavent, Bauer, Neumann, & Friese, 2013). In addition, the blockade of the neutrophil-
397 specific chemokine receptor CXCR2 renders mice resistant to EAE (Carlson, Kroenke, Rao, Lane, &
398 Segal, 2008). Our results show that neutrophil granulocytes were among the recruited immune cells, for
399 which the stimulation of has been shown to promote EAE (Kilic et al., 2015). Thus, it is believed that
400 granulocytes are important contributors in preparing for CNS inflammation by priming microglia and
401 inducing their maturation (Steinbach et al., 2013). Whereas we observed low granulocyte numbers in
402 the peripheral blood of control and cuprizone-treated animals, high numbers were observed in the blood
403 of EAE and Cup/EAE mice as well as in the forebrains of Cup/EAE mice. Nevertheless, the relevance
404 of these cells for inflammatory forebrain lesion development in Cup/EAE mice remains to be clarified.

405 One important question is which factor(s) triggers granulocyte recruitment into the forebrain. It
406 is well known that the development of Th17 cells is a key event in the pathogenesis of MOG₃₅₋₅₅-induced
407 EAE (Cua et al., 2003; Park et al., 2005; Serada et al., 2008), and adoptively transferred CD4⁺ T cells
408 secreting IL-17, the signature Th17 cytokine, migrate into the corpus callosa of cuprizone-fed mice
409 (Baxi et al., 2015). IL-17 induces neutrophil-mobilizing/activating factors, including chemokines that
410 target granulocytes, such as CXCL1, CXCL2, and CXCL5 (Iwakura, Ishigame, Saijo, & Nakae, 2011).
411 Brain-intrinsic synthesis of IL-17 has been shown to promote granulocyte infiltration and aggravate
412 myelin loss and behavioral deficits in the cuprizone model (Zimmermann et al., 2017). This suggests
413 that Th17 lymphocytes infiltrate the forebrain in our Cup/EAE model and recruit granulocytes. Along
414 this line, neutrophils that infiltrate the CNS may secrete soluble factors—most likely several
415 proinflammatory proteins—that contribute to the maturation of antigen-presenting cells and affect the
416 reactivation of myelin antigen-specific T cells. Indeed, it was shown that bone marrow-derived dendritic
417 cells exposed to neutrophils from EAE spinal cord express MHC class II and the costimulatory
418 molecules CD80 and CD86 (Steinbach et al., 2013), thus potentially increasing their capacity to
419 restimulate effector T cells. Further studies are needed to determine whether recruited granulocytes in
420 the Cup/EAE model are able to activate microglia and enhance their capacity to restimulate effector T
421 cells in a similar manner.

422 A final important observation from this study was that the forebrain lesions in Cup/EAE mice
423 are self-limiting (i.e. show spontaneous resolution), whereas lesions located in the spinal cord are not.
424 The reason for this discrepancy is currently unclear. However, a detailed comparison of spinal cord and
425 forebrain lesions at the molecular and cellular levels will help to elucidate the factors potentially
426 involved in inflammatory lesion progression and/or resolution.

427 In summary, our findings add to our understanding of the Cup/EAE model, a practical and
428 effective tool for studying immune cell recruitment in MS. Of note, the model has great translational
429 potential, as most imaging and pathological MS studies are performed in the forebrain. By contrast, most
430 EAE studies focus on spinal cord lesions. The presented Cup/EAE model will provide valuable insight
431 into inflammatory lesion development and progression in the forebrain.

432

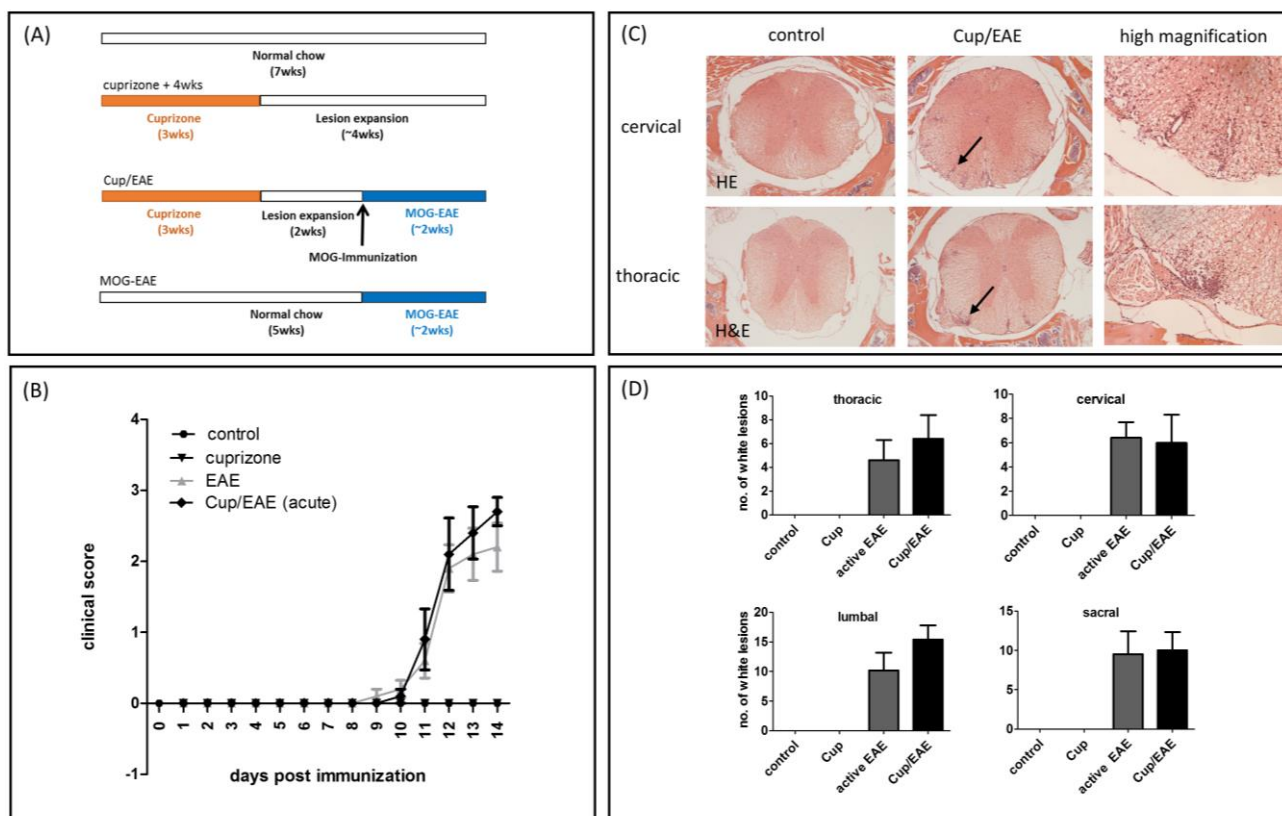
433 **Acknowledgements**

434 This study was supported by the Dr. Robert Pflieger Stiftung (M.K.). The technical support from P. Ibold,
435 H. Helten, S. Wübbel, B. Aschauer, and A. Baltruschat is acknowledged.

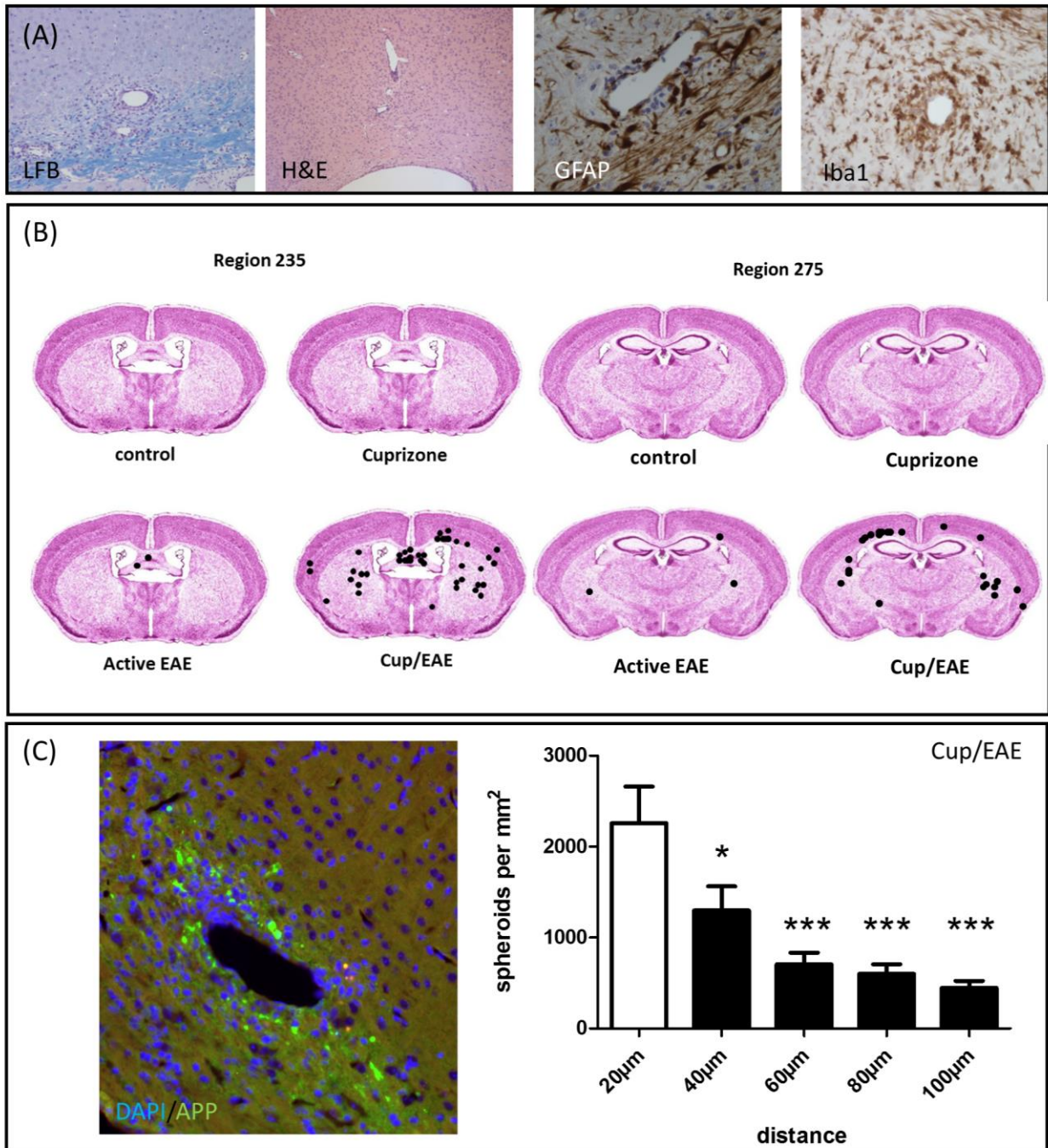
436

437 **Conflict of interest:**

438 The authors declare no competing financial interests.

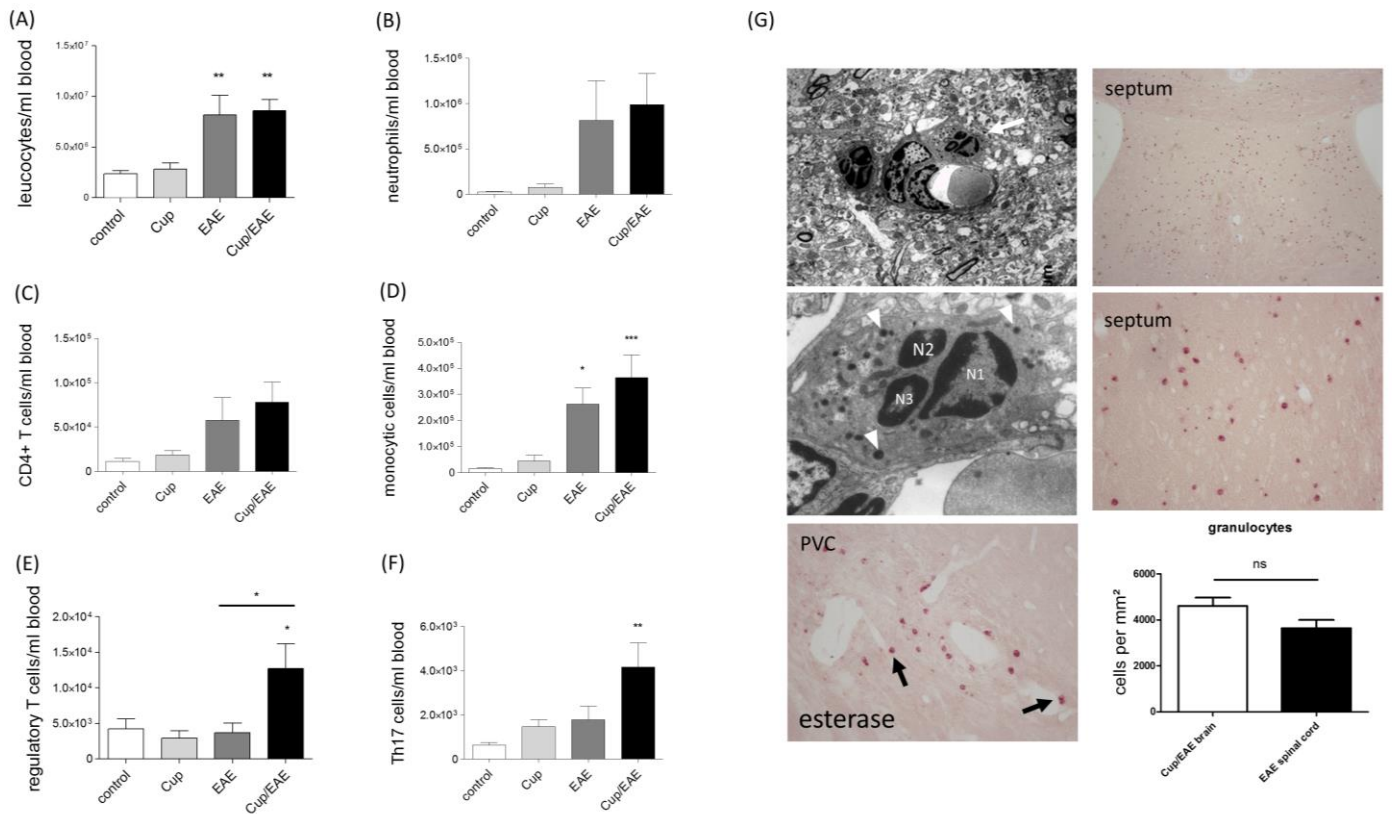
440 **Figure 1. Clinical disease progression.**

441 (A) Schematic depicting the experimental setup. Periods of cuprizone intoxication are highlighted in
 442 orange, whereas periods of MOG₃₅₋₅₅ immunization and subsequent active EAE development are
 443 highlighted in blue. (B) Clinical scores for control, EAE, and Cup/EAE mice. (C) Representative H&E-
 444 stained spinal cord sections from control and Cup/EAE mice. Images at higher magnification are regions
 445 indicated by arrows in Cup/EAE images. (D) Quantification of inflammatory infiltrates in spinal cords
 446 at different levels.



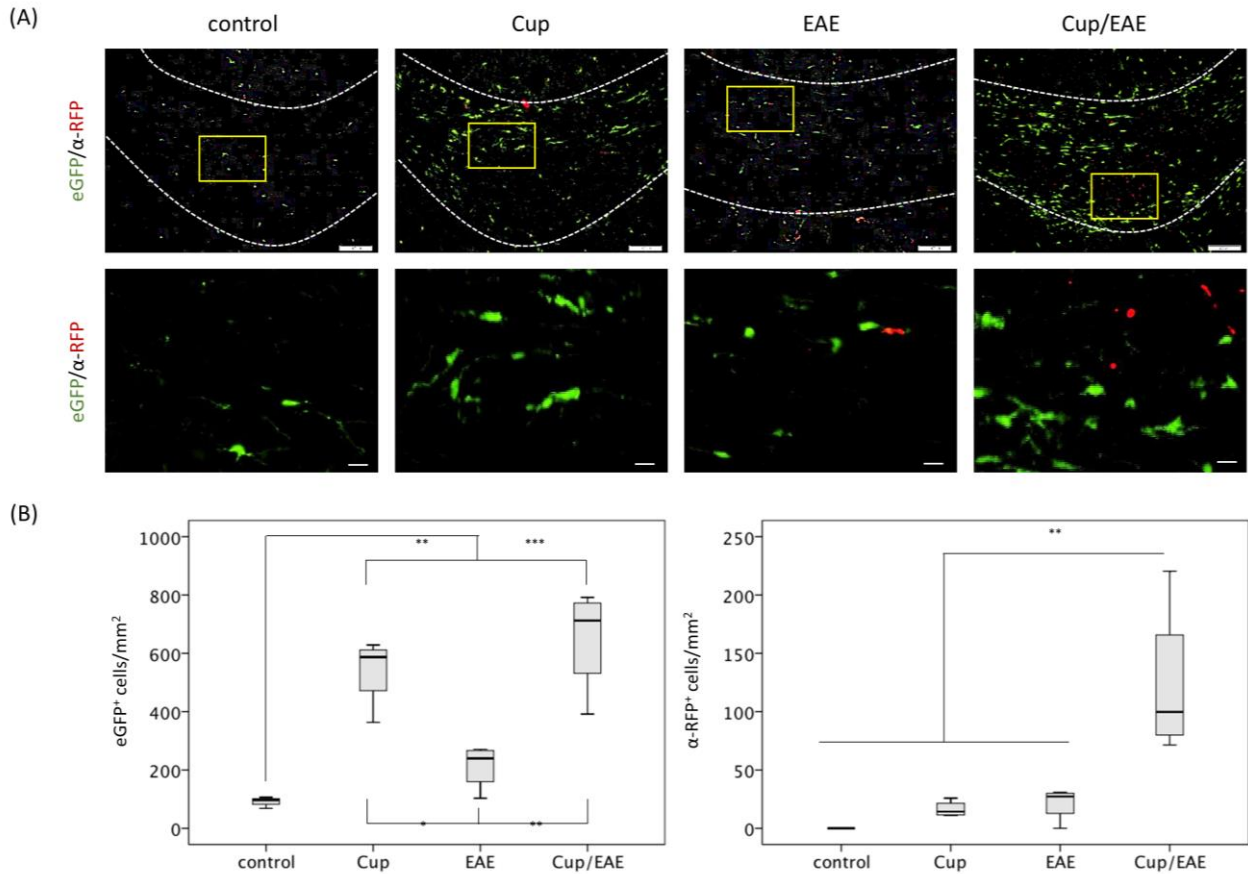
447 **Figure 2. Forebrain inflammatory cell infiltration.**

448 (A) Histopathological characteristics of inflammatory forebrain lesions in Cup/EAE mice. Immune cell
 449 neuropil invasion induces focal demyelination (shown with LFB), which is paralleled by the breakdown
 450 of the glia limitans perivascularis (shown with GFAP immunoreactivity) and accumulation of
 451 microglia/monocytes (shown with Iba1 immunoreactivity). (B) Distribution of perivascular infiltrates
 452 in the different treatment groups (H&E staining; black dots from one independent observer) at two brain
 453 levels (regions according to Sidman et al.). (C) Perivascular acute axonal injury visualized by anti-APP
 454 immunohistochemistry. APP⁺ spheroid density was determined in concentric areas (up to 100 μm)
 455 from the vessel center. Differences determined using one-way ANOVA with Dunnett's post-hoc test; **p* <
 456 0.05 and ****p* < 0.001 vs. 20 μm.



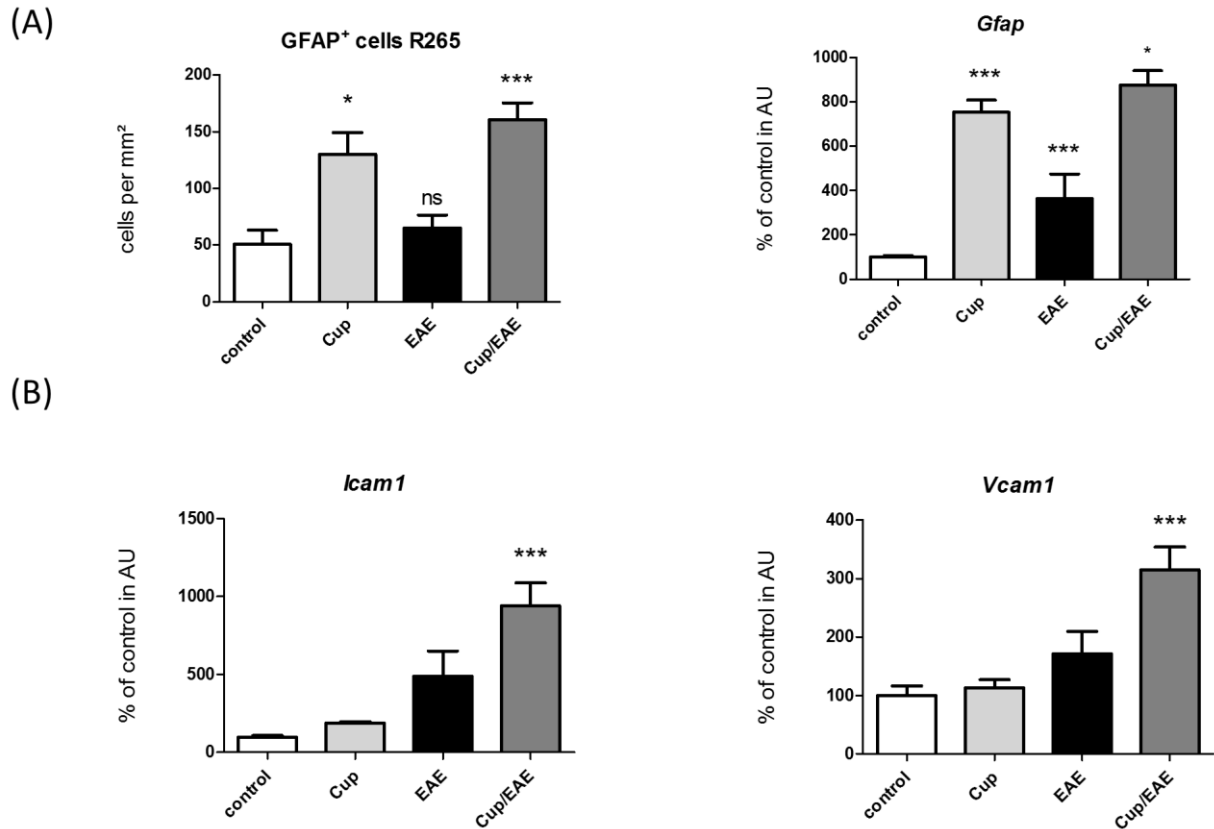
457 **Figure 3. Peripheral inflammatory response.**

458 (A–F) Absolute cell numbers were determined in peripheral blood samples of control, Cup, EAE, and
 459 Cup/EAE mice. Numbers of total leucocytes (determined via CountBright Beads; Molecular Probes)
 460 (A), neutrophil granulocytes (Ly6G⁺F4/80⁺) (B), Th lymphocytes (CD4⁺) (C), monocytes (F4/80⁺) (D),
 461 regulatory T lymphocytes (CD4⁺CD25⁺FOXP3⁺) (E), and Th17 lymphocytes (CD4⁺IL17⁺) (F).
 462 Differences between groups determined using one-way ANOVAs with Dunnett’s post-hoc tests; **p* <
 463 0.05, ***p* < 0.01, and ****p* < 0.001 vs. control. (G) Ultrastructural imaging (upper, middle left) of
 464 infiltrating neutrophils. Note the segmented nucleus (N1–N3) as well as numerous lysosomes
 465 (arrowheads). Naphthol AS-D chloroacetate (esterase) staining (bottom left) revealed granulocytes (pink
 466 cells; arrows) around vessels and within the neuropil. (bottom right) Similar densities of neutrophils
 467 were detected in inflammatory forebrain infiltrates of Cup/EAE mice and in spinal cord infiltrates in
 468 EAE mice.



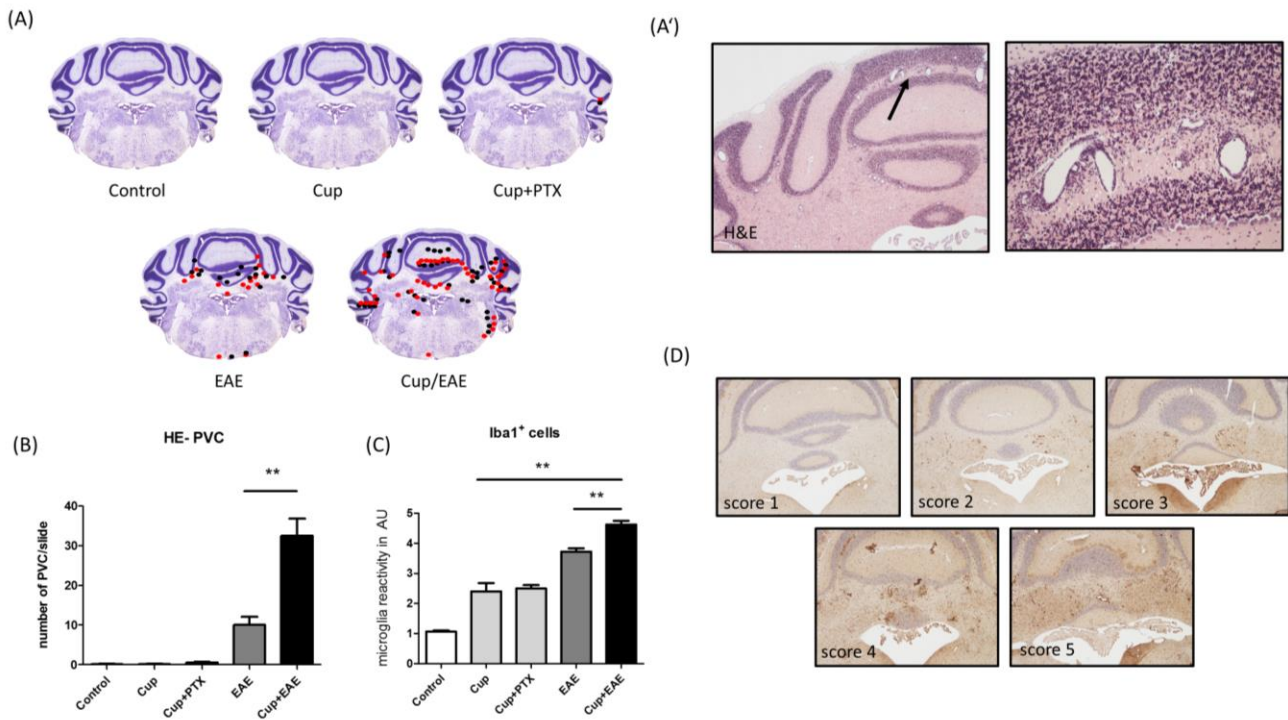
469 **Figure 4. Monocyte recruitment in Cup/EAE mice.**

470 (A) Representative images of the splenia of the corpus callosa (delineated by dotted lines) from control,
 471 Cup, EAE, and Cup/EAE mice showing microglia (green) and infiltrating monocytes (red). The Scale
 472 bars indicate 100 μm (top) and 10 μm (bottom). (B) Microglia and macrophage densities within the
 473 splenia of the corpus callosa from control ($n = 3$), Cup ($n = 4$), EAE ($n = 4$), and Cup/EAE ($n = 4$) mice;
 474 $*p < 0.05$, $**p < 0.01$, and $***p < 0.001$ via one-way ANOVAs with Tukey's post-hoc tests.



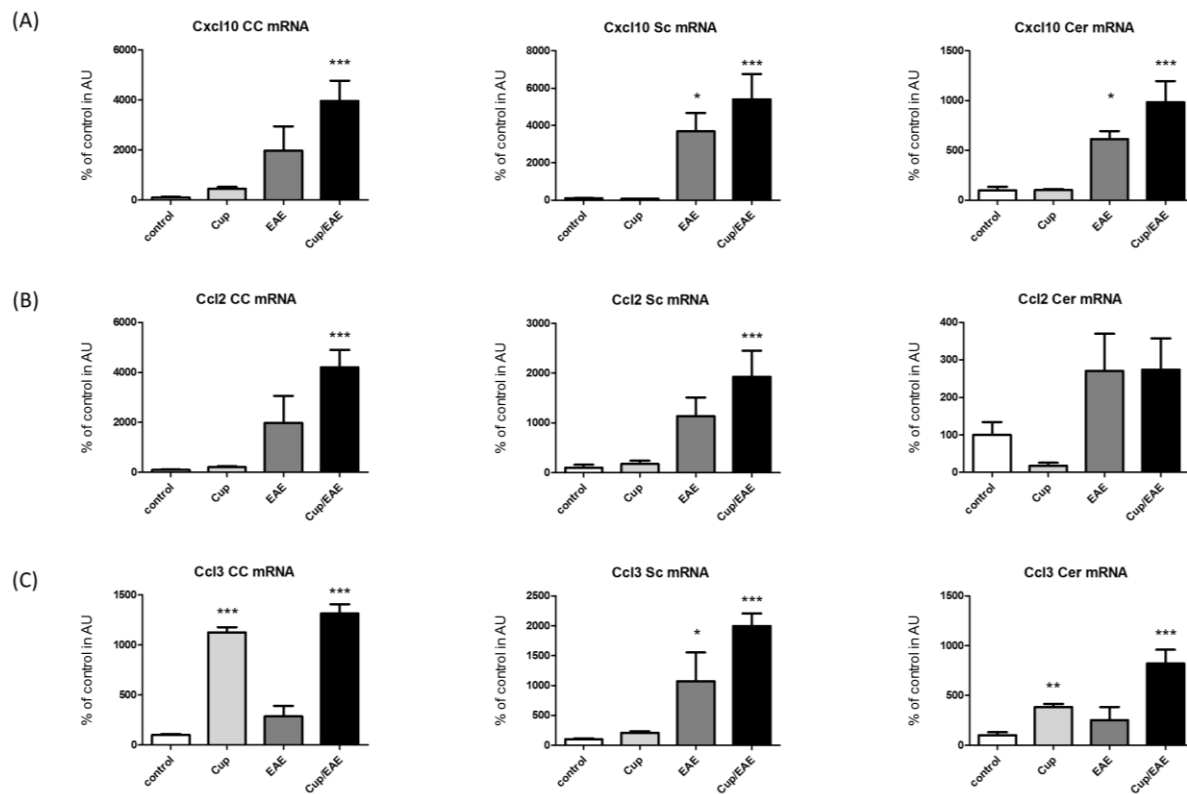
475 **Figure 5. Induction of cell adhesion molecules in Cup/EAE mice.**

476 (A) Quantification of GFAP⁺ astrocytes and *Gfap* mRNA levels in medial parts of the corpus callosum
 477 show similar inductions in Cup and Cup/EAE treatment groups. (B) mRNA expression levels of
 478 intercellular adhesion molecule 1 (*Icam1*) and vascular cell adhesion molecule 1 (*Vcam1*) in control (n
 479 = 5), Cup ($n = 5$), EAE ($n = 4$), and Cup/EAE ($n = 5$) mice; * $p < 0.05$ and *** $p < 0.001$ vs. controls via
 480 one-way ANOVAs with Dunnett's post-hoc test. ns, not significant.



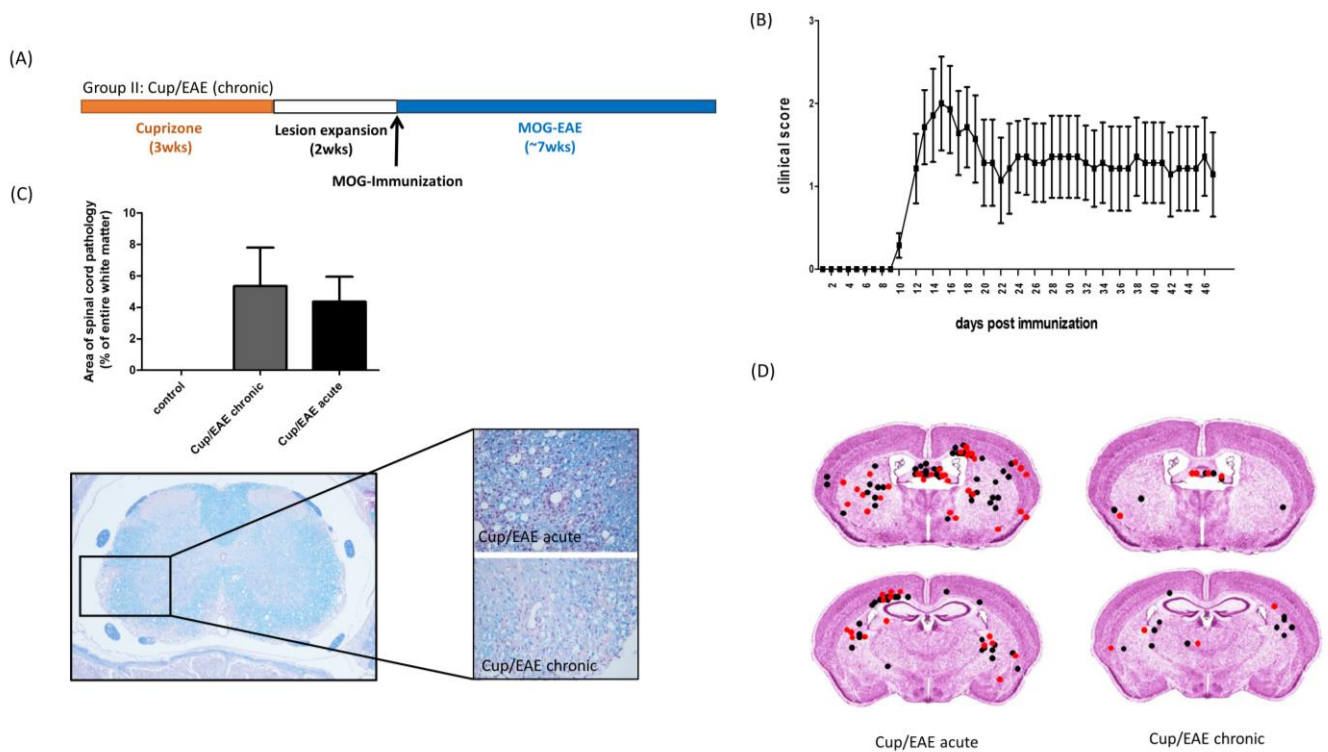
481 **Figure 6. Cerebellar inflammatory cell infiltration.**

482 (A) Spatial distribution of loci of perivascular infiltrates (red and black dots from two independent
 483 observers) in cerebella. (A') Representative images of perivascular infiltrates in the cerebellum (H&E
 484 staining). (B) Number of perivascular infiltrates in different treatment groups. (C,D) The extent of
 485 microglia/monocyte activation was determined by blinded scoring (1, normal; 5, maximum activity; see
 486 panel D for representative images) of Iba1 immunoreactivity; * $p < 0.05$, ** $p < 0.01$, and *** $p < 0.001$
 487 via Mann Whitney tests.



488 **Figure 7. Chemokine expression.**

489 mRNA expression levels of the chemokines C-X-C motif ligand 10 (*Cxcl10*) (A), C-C motif ligand 2
 490 (*Ccl2*) (B), and C-C motif ligand 3 (*Ccl3*) (C) in the corpus callosum (CC), spinal cord (Sc) and
 491 cerebellum (Cer). Comparisons of the mRNA levels between control ($n = 5$), Cup ($n = 5$), EAE ($n = 4$),
 492 and Cup/EAE ($n = 5$) mice were conducted using one-way ANOVAs with Dunnett's post-hoc tests; * p
 493 < 0.05, ** p < 0.01, and *** p < 0.001 vs. control.



494 **Figure 8. Lesions during the chronic disease stage in Cup/EAE mice.**

495 (A) Schematic depicting the experimental setup. Period of cuprizone intoxication is highlighted in
 496 orange, whereas the period for MOG₃₅₋₅₅ immunization and subsequent active EAE development is
 497 highlighted in blue. (B) Clinical scores of Cup/EAE (chronic) mice. (C) Spinal cord pathology in
 498 Cup/EAE mice during acute and chronic stages (LFB/periodic acid-Schiff staining). (D) Distribution of
 499 perivascular infiltrates in the forebrains of Cup/EAE mice during acute and chronic stages (H&E
 500 staining). Analysis was performed by two independent observers (red and black dots).

501 **References**

- 502 Acs, P., Kipp, M., Norkute, A., Johann, S., Clarner, T., Braun, A., . . . Beyer, C. (2009). 17beta-estradiol
503 and progesterone prevent cuprizone provoked demyelination of corpus callosum in male
504 mice. *Glia*, *57*(8), 807-814. doi:10.1002/glia.20806
- 505 Alvarez, J. I., Katayama, T., & Prat, A. (2013). Glial influence on the blood brain barrier. *Glia*, *61*(12),
506 1939-1958. doi:10.1002/glia.22575
- 507 Aube, B., Levesque, S. A., Pare, A., Chamma, E., Kebir, H., Gorina, R., . . . Lacroix, S. (2014).
508 Neutrophils mediate blood-spinal cord barrier disruption in demyelinating
509 neuroinflammatory diseases. *J Immunol*, *193*(5), 2438-2454. doi:10.4049/jimmunol.1400401
- 510 Bakker, D. A., & Ludwin, S. K. (1987). Blood-brain barrier permeability during Cuprizone-induced
511 demyelination. Implications for the pathogenesis of immune-mediated demyelinating
512 diseases. *J Neurol Sci*, *78*(2), 125-137.
- 513 Barnett, M. H., & Prineas, J. W. (2004). Relapsing and remitting multiple sclerosis: pathology of the
514 newly forming lesion. *Ann Neurol*, *55*(4), 458-468. doi:10.1002/ana.20016
- 515 Bauer, J., Rauschka, H., & Lassmann, H. (2001). Inflammation in the nervous system: the human
516 perspective. *Glia*, *36*(2), 235-243.
- 517 Baxi, E. G., DeBruin, J., Tosi, D. M., Grishkan, I. V., Smith, M. D., Kirby, L. A., . . . Gocke, A. R. (2015).
518 Transfer of myelin-reactive th17 cells impairs endogenous remyelination in the central
519 nervous system of cuprizone-fed mice. *J Neurosci*, *35*(22), 8626-8639.
520 doi:10.1523/jneurosci.3817-14.2015
- 521 Benn, T., Halfpenny, C., & Scolding, N. (2001). Glial cells as targets for cytotoxic immune mediators.
522 *Glia*, *36*(2), 200-211.
- 523 Berghoff, S. A., Gerndt, N., Winchenbach, J., Stumpf, S. K., Hosang, L., Odoardi, F., . . . Saher, G.
524 (2017). Dietary cholesterol promotes repair of demyelinated lesions in the adult brain. *Nat*
525 *Commun*, *8*, 14241. doi:10.1038/ncomms14241
- 526 Bitsch, A., Schuchardt, J., Bunkowski, S., Kuhlmann, T., & Bruck, W. (2000). Acute axonal injury in
527 multiple sclerosis. Correlation with demyelination and inflammation. *Brain*, *123* (Pt 6), 1174-
528 1183.
- 529 Boretius, S., Escher, A., Dallenga, T., Wrzos, C., Tammer, R., Bruck, W., . . . Stadelmann, C. (2012).
530 Assessment of lesion pathology in a new animal model of MS by multiparametric MRI and
531 DTI. *Neuroimage*, *59*(3), 2678-2688. doi:10.1016/j.neuroimage.2011.08.051
- 532 Carlson, T., Kroenke, M., Rao, P., Lane, T. E., & Segal, B. (2008). The Th17-ELR+ CXC chemokine
533 pathway is essential for the development of central nervous system autoimmune disease. *J*
534 *Exp Med*, *205*(4), 811-823. doi:10.1084/jem.20072404
- 535 Carr, M. W., Roth, S. J., Luther, E., Rose, S. S., & Springer, T. A. (1994). Monocyte chemoattractant
536 protein 1 acts as a T-lymphocyte chemoattractant. *Proc Natl Acad Sci U S A*, *91*(9), 3652-
537 3656.
- 538 Charcot, M. (1868). Histologie de la sclerose en plaque. *Gaz. Hosp*, *41*, 554-556.
- 539 Clarner, T., Diederichs, F., Berger, K., Denecke, B., Gan, L., van der Valk, P., . . . Kipp, M. (2012). Myelin
540 debris regulates inflammatory responses in an experimental demyelination animal model
541 and multiple sclerosis lesions. *Glia*, *60*(10), 1468-1480. doi:10.1002/glia.22367
- 542 Clarner, T., Janssen, K., Nellessen, L., Stangel, M., Skripuletz, T., Krauspe, B., . . . Kipp, M. (2015).
543 CXCL10 triggers early microglial activation in the cuprizone model. *J Immunol*, *194*(7), 3400-
544 3413. doi:10.4049/jimmunol.1401459
- 545 Codarri, L., Greter, M., & Becher, B. (2013). Communication between pathogenic T cells and myeloid
546 cells in neuroinflammatory disease. *Trends Immunol*, *34*(3), 114-119.
547 doi:10.1016/j.it.2012.09.007
- 548 Cua, D. J., Sherlock, J., Chen, Y., Murphy, C. A., Joyce, B., Seymour, B., . . . Sedgwick, J. D. (2003).
549 Interleukin-23 rather than interleukin-12 is the critical cytokine for autoimmune
550 inflammation of the brain. *Nature*, *421*(6924), 744-748. doi:10.1038/nature01355
- 551 Dooley, D., Lemmens, E., Vanganswinkel, T., Le Blon, D., Hoornaert, C., Ponsaerts, P., & Hendrix, S.
552 (2016). Cell-Based Delivery of Interleukin-13 Directs Alternative Activation of Macrophages

553 Resulting in Improved Functional Outcome after Spinal Cord Injury. *Stem Cell Reports*, 7(6),
554 1099-1115. doi:10.1016/j.stemcr.2016.11.005

555 Gehrmann, J., Banati, R. B., Cuzner, M. L., Kreutzberg, G. W., & Newcombe, J. (1995). Amyloid
556 precursor protein (APP) expression in multiple sclerosis lesions. *Glia*, 15(2), 141-151.
557 doi:10.1002/glia.440150206

558 Glad, S. B., Nyland, H. I., Aarseth, J. H., Riise, T., & Myhr, K. M. (2009). Long-term follow-up of benign
559 multiple sclerosis in Hordaland County, Western Norway. *Mult Scler*, 15(8), 942-950.
560 doi:10.1177/1352458509106511

561 Groebe, A., Clarner, T., Baumgartner, W., Dang, J., Beyer, C., & Kipp, M. (2009). Cuprizone treatment
562 induces distinct demyelination, astrogliosis, and microglia cell invasion or proliferation in the
563 mouse cerebellum. *Cerebellum*, 8(3), 163-174. doi:10.1007/s12311-009-0099-3

564 Hartung, H. P., Aktas, O., Menge, T., & Kieseier, B. C. (2014). Immune regulation of multiple sclerosis.
565 *Handb Clin Neurol*, 122, 3-14. doi:10.1016/b978-0-444-52001-2.00001-7

566 Hertwig, L., Pache, F., Romero-Suarez, S., Stürner, K. H., Borisow, N., Behrens, J., . . . Paul, F. (2016).
567 Distinct functionality of neutrophils in multiple sclerosis and neuromyelitis optica. *Mult Scler*,
568 22(2), 160-173. doi:10.1177/1352458515586084

569 Hiremath, M. M., Chen, V. S., Suzuki, K., Ting, J. P., & Matsushima, G. K. (2008). MHC class II
570 exacerbates demyelination in vivo independently of T cells. *J Neuroimmunol*, 203(1), 23-32.
571 doi:10.1016/j.jneuroim.2008.06.034

572 Hoflich, K. M., Beyer, C., Clarner, T., Schmitz, C., Nyamoya, S., Kipp, M., & Hochstrasser, T. (2016).
573 Acute axonal damage in three different murine models of multiple sclerosis: A comparative
574 approach. *Brain Res*, 1650, 125-133. doi:10.1016/j.brainres.2016.08.048

575 Iglesias, A., Bauer, J., Litznerberger, T., Schubart, A., & Lington, C. (2001). T- and B-cell responses to
576 myelin oligodendrocyte glycoprotein in experimental autoimmune encephalomyelitis and
577 multiple sclerosis. *Glia*, 36(2), 220-234.

578 Iwakura, Y., Ishigame, H., Saijo, S., & Nakae, S. (2011). Functional specialization of interleukin-17
579 family members. *Immunity*, 34(2), 149-162. doi:10.1016/j.immuni.2011.02.012

580 Kilic, A. K., Esendagli, G., Sayat, G., Talim, B., Karabudak, R., & Kurne, A. T. (2015). Promotion of
581 experimental autoimmune encephalomyelitis upon neutrophil granulocytes' stimulation with
582 formyl-methionyl-leucyl-phenylalanine (fMLP) peptide. *Autoimmunity*, 48(6), 423-428.
583 doi:10.3109/08916934.2015.1030615

584 Kondo, A., Nakano, T., & Suzuki, K. (1987). Blood-brain barrier permeability to horseradish peroxidase
585 in twitcher and cuprizone-intoxicated mice. *Brain Res*, 425(1), 186-190.

586 Korn, T., Reddy, J., Gao, W., Bettelli, E., Awasthi, A., Petersen, T. R., . . . Kuchroo, V. K. (2007). Myelin-
587 specific regulatory T cells accumulate in the CNS but fail to control autoimmune
588 inflammation. *Nat Med*, 13(4), 423-431. doi:10.1038/nm1564

589 Kornek, B., Storch, M. K., Weissert, R., Wallstroem, E., Stefferl, A., Olsson, T., . . . Lassmann, H. (2000).
590 Multiple sclerosis and chronic autoimmune encephalomyelitis: a comparative quantitative
591 study of axonal injury in active, inactive, and remyelinated lesions. *Am J Pathol*, 157(1), 267-
592 276. doi:10.1016/s0002-9440(10)64537-3

593 Kuerten, S., Kostova-Bales, D. A., Frenzel, L. P., Tigno, J. T., Tary-Lehmann, M., Angelov, D. N., &
594 Lehmann, P. V. (2007). MP4- and MOG:35-55-induced EAE in C57BL/6 mice differentially
595 targets brain, spinal cord and cerebellum. *J Neuroimmunol*, 189(1-2), 31-40.
596 doi:10.1016/j.jneuroim.2007.06.016

597 Kuhlmann, T., Lingfeld, G., Bitsch, A., Schuchardt, J., & Bruck, W. (2002). Acute axonal damage in
598 multiple sclerosis is most extensive in early disease stages and decreases over time. *Brain*,
599 125(Pt 10), 2202-2212.

600 Le Blon, D., Guglielmetti, C., Hoornaert, C., Quarta, A., Daans, J., Dooley, D., . . . Ponsaerts, P. (2016).
601 Intracerebral transplantation of interleukin 13-producing mesenchymal stem cells limits
602 microgliosis, oligodendrocyte loss and demyelination in the cuprizone mouse model. *J*
603 *Neuroinflammation*, 13(1), 288. doi:10.1186/s12974-016-0756-7

604 Liu, K. K., & Dorovini-Zis, K. (2012). Differential regulation of CD4+ T cell adhesion to cerebral
605 microvascular endothelium by the beta-chemokines CCL2 and CCL3. *Int J Mol Sci*, *13*(12),
606 16119-16140. doi:10.3390/ijms131216119

607 Liu, L., Belkadi, A., Darnall, L., Hu, T., Drescher, C., Cotleur, A. C., . . . Ransohoff, R. M. (2010). CXCR2-
608 positive neutrophils are essential for cuprizone-induced demyelination: relevance to multiple
609 sclerosis. *Nat Neurosci*, *13*(3), 319-326. doi:10.1038/nn.2491

610 Liu, Y., Holdbrooks, A. T., Meares, G. P., Buckley, J. A., Benveniste, E. N., & Qin, H. (2015). Preferential
611 Recruitment of Neutrophils into the Cerebellum and Brainstem Contributes to the Atypical
612 Experimental Autoimmune Encephalomyelitis Phenotype. *J Immunol*, *195*(3), 841-852.
613 doi:10.4049/jimmunol.1403063

614 Lublin, F. D., Reingold, S. C., Cohen, J. A., Cutter, G. R., Sorensen, P. S., Thompson, A. J., . . . Polman, C.
615 H. (2014). Defining the clinical course of multiple sclerosis: the 2013 revisions. *Neurology*,
616 *83*(3), 278-286. doi:10.1212/wnl.0000000000000560

617 Lucchinetti, C., Bruck, W., Parisi, J., Scheithauer, B., Rodriguez, M., & Lassmann, H. (2000).
618 Heterogeneity of multiple sclerosis lesions: implications for the pathogenesis of
619 demyelination. *Ann Neurol*, *47*(6), 707-717.

620 McGeachy, M. J., Stephens, L. A., & Anderton, S. M. (2005). Natural recovery and protection from
621 autoimmune encephalomyelitis: contribution of CD4+CD25+ regulatory cells within the
622 central nervous system. *J Immunol*, *175*(5), 3025-3032.

623 McMahan, E. J., Suzuki, K., & Matsushima, G. K. (2002). Peripheral macrophage recruitment in
624 cuprizone-induced CNS demyelination despite an intact blood-brain barrier. *J Neuroimmunol*,
625 *130*(1-2), 32-45.

626 Mildner, A., Schmidt, H., Nitsche, M., Merkler, D., Hanisch, U. K., Mack, M., . . . Prinz, M. (2007).
627 Microglia in the adult brain arise from Ly-6ChiCCR2+ monocytes only under defined host
628 conditions. *Nat Neurosci*, *10*(12), 1544-1553. doi:10.1038/nn2015

629 Millward, J. M., Caruso, M., Campbell, I. L., Gaudie, J., & Owens, T. (2007). IFN-gamma-induced
630 chemokines synergize with pertussis toxin to promote T cell entry to the central nervous
631 system. *J Immunol*, *178*(12), 8175-8182.

632 Moreno, M., Bannerman, P., Ma, J., Guo, F., Miers, L., Soulika, A. M., & Pleasure, D. (2014).
633 Conditional ablation of astroglial CCL2 suppresses CNS accumulation of M1 macrophages and
634 preserves axons in mice with MOG peptide EAE. *J Neurosci*, *34*(24), 8175-8185.
635 doi:10.1523/jneurosci.1137-14.2014

636 Noell, S., Wolburg-Buchholz, K., Mack, A. F., Ritz, R., Tatagiba, M., Beschoner, R., . . . Fallier-Becker,
637 P. (2012). Dynamics of expression patterns of AQP4, dystroglycan, agrin and matrix
638 metalloproteinases in human glioblastoma. *Cell Tissue Res*, *347*(2), 429-441.
639 doi:10.1007/s00441-011-1321-4

640 Norkute, A., Hieble, A., Braun, A., Johann, S., Clarner, T., Baumgartner, W., . . . Kipp, M. (2009).
641 Cuprizone treatment induces demyelination and astrocytosis in the mouse hippocampus. *J*
642 *Neurosci Res*, *87*(6), 1343-1355. doi:10.1002/jnr.21946

643 Nunes, J. C., Radbruch, H., Walz, R., Lin, K., Stenzel, W., Prokop, S., . . . Heppner, F. L. (2015). The
644 most fulminant course of the Marburg variant of multiple sclerosis-autopsy findings. *Mult*
645 *Scler*, *21*(4), 485-487. doi:10.1177/1352458514537366

646 Park, H., Li, Z., Yang, X. O., Chang, S. H., Nurieva, R., Wang, Y. H., . . . Dong, C. (2005). A distinct
647 lineage of CD4 T cells regulates tissue inflammation by producing interleukin 17. *Nat*
648 *Immunol*, *6*(11), 1133-1141. doi:10.1038/ni1261

649 Pfeifenbring, S., Bunyan, R. F., Metz, I., Rover, C., Huppke, P., Gartner, J., . . . Bruck, W. (2015).
650 Extensive acute axonal damage in pediatric multiple sclerosis lesions. *Ann Neurol*, *77*(4), 655-
651 667. doi:10.1002/ana.24364

652 Pierson, E. R., Wagner, C. A., & Goverman, J. M. (2016). The contribution of neutrophils to CNS
653 autoimmunity. *Clin Immunol*. doi:10.1016/j.clim.2016.06.017

654 Price, P. J., Luckow, B., Torres-Dominguez, L. E., Brandmuller, C., Zorn, J., Kirschning, C. J., . . .
655 Lehmann, M. H. (2014). Chemokine (C-C Motif) receptor 1 is required for efficient

656 recruitment of neutrophils during respiratory infection with modified vaccinia virus Ankara. *J*
657 *Virol*, 88(18), 10840-10850. doi:10.1128/jvi.01524-14

658 Rush, C. A., MacLean, H. J., & Freedman, M. S. (2015). Aggressive multiple sclerosis: proposed
659 definition and treatment algorithm. *Nat Rev Neurol*, 11(7), 379-389.
660 doi:10.1038/nrneurol.2015.85

661 Saederup, N., Cardona, A. E., Croft, K., Mizutani, M., Cotleur, A. C., Tsou, C. L., . . . Charo, I. F. (2010).
662 Selective chemokine receptor usage by central nervous system myeloid cells in CCR2-red
663 fluorescent protein knock-in mice. *PLoS One*, 5(10), e13693.
664 doi:10.1371/journal.pone.0013693

665 Sartori, A., Abdoli, M., & Freedman, M. S. (2017). Can we predict benign multiple sclerosis? Results of
666 a 20-year long-term follow-up study. *J Neurol*, 264(6), 1068-1075. doi:10.1007/s00415-017-
667 8487-y

668 Scheld, M., Ruther, B. J., Grosse-Veldmann, R., Ohl, K., Tenbrock, K., Dreytmüller, D., . . . Kipp, M.
669 (2016). Neurodegeneration Triggers Peripheral Immune Cell Recruitment into the Forebrain.
670 *J Neurosci*, 36(4), 1410-1415. doi:10.1523/jneurosci.2456-15.2016

671 Schirmer, L., Merkler, D., König, F. B., Brück, W., & Stadelmann, C. (2013). Neuroaxonal regeneration
672 is more pronounced in early multiple sclerosis than in traumatic brain injury lesions. *Brain*
673 *Pathol*, 23(1), 2-12. doi:10.1111/j.1750-3639.2012.00608.x

674 Serada, S., Fujimoto, M., Mihara, M., Koike, N., Ohsugi, Y., Nomura, S., . . . Naka, T. (2008). IL-6
675 blockade inhibits the induction of myelin antigen-specific Th17 cells and Th1 cells in
676 experimental autoimmune encephalomyelitis. *Proceedings of the National Academy of*
677 *Sciences of the United States of America*, 105(26), 9041-9046. doi:10.1073/pnas.0802218105

678 Skripuletz, T., Bussmann, J. H., Gudi, V., Koutsoudaki, P. N., Pul, R., Moharreh-Khiabani, D., . . .
679 Stangel, M. (2010). Cerebellar cortical demyelination in the murine cuprizone model. *Brain*
680 *Pathol*, 20(2), 301-312. doi:10.1111/j.1750-3639.2009.00271.x

681 Slowik, A., Schmidt, T., Beyer, C., Amor, S., Clarner, T., & Kipp, M. (2015). The sphingosine 1-
682 phosphate receptor agonist FTY720 is neuroprotective after cuprizone-induced CNS
683 demyelination. *Br J Pharmacol*, 172(1), 80-92. doi:10.1111/bph.12938

684 Steinbach, K., Piedavent, M., Bauer, S., Neumann, J. T., & Friese, M. A. (2013). Neutrophils amplify
685 autoimmune central nervous system infiltrates by maturing local APCs. *J Immunol*, 191(9),
686 4531-4539. doi:10.4049/jimmunol.1202613

687 Trapp, B. D., Ransohoff, R., & Rudick, R. (1999). Axonal pathology in multiple sclerosis: relationship to
688 neurologic disability. *Curr Opin Neurol*, 12(3), 295-302.

689 Werner, K., Bitsch, A., Bunkowski, S., Hemmerlein, B., & Brück, W. (2002). The relative number of
690 macrophages/microglia expressing macrophage colony-stimulating factor and its receptor
691 decreases in multiple sclerosis lesions. *Glia*, 40(1), 121-129. doi:10.1002/glia.10120

692 Wu, F., Cao, W., Yang, Y., & Liu, A. (2010). Extensive infiltration of neutrophils in the acute phase of
693 experimental autoimmune encephalomyelitis in C57BL/6 mice. *Histochem Cell Biol*, 133(3),
694 313-322. doi:10.1007/s00418-009-0673-2

695 Xu, L. L., Warren, M. K., Rose, W. L., Gong, W., & Wang, J. M. (1996). Human recombinant monocyte
696 chemotactic protein and other C-C chemokines bind and induce directional migration of
697 dendritic cells in vitro. *J Leukoc Biol*, 60(3), 365-371.

698 Zimmermann, J., Emrich, M., Krauthausen, M., Saxe, S., Nitsch, L., Heneka, M. T., . . . Müller, M.
699 (2017). IL-17A Promotes Granulocyte Infiltration, Myelin Loss, Microglia Activation, and
700 Behavioral Deficits During Cuprizone-Induced Demyelination. *Mol Neurobiol*.
701 doi:10.1007/s12035-016-0368-3